A SENSOR SYSTEM DESIGNED FOR ELECTROCHEMICAL IMPEDANCE SPECTROSCOPE-BASED COATING PERFORMANCE EVALUATION

A Thesis
Submitted to the Graduate Faculty
of the
North Dakota State University
of Agriculture and Applied Science

By

Yulong Shi

In Partial Fulfillment of the Requirements
for the Degree of
MASTER OF SCIENCE

Major Department:
Electrical and Computer Engineering

May 2010

Fargo, North Dakota

North Dakota State University
Graduate School

Title

A SENSOR SYSTEM DESIGNED FOR ELECTROCHEMICAL IMPEDANCE

SPECTROSCOPE-BASED COATING PERFORMANCE EVALUATION

By

Yulong Shi

The Supervisory Committee certifies that this *disquisition* complies with North Dakota State University's regulations and meets the accepted standards for the degree of

MASTER OF SCIENCE

ABSTRACT

Shi, Yulong, M.S., Department of Electrical and Computer Engineering, College of Engineering and Architecture, North Dakota State University, May 2010. A Sensor System Designed for Electrochemical Impedance Spectroscope-based Coating Performance Evaluation. Major Professor: Chao You.

●ne of the traditional methods for coating performance evaluation is using Electrochemical Impedance Spectroscopy (EIS). The theory of using EIS to evaluate coating performance is to measure the coating impedance in a frequency range of 0.01 Hz to 100 KHz. Based on the observation of a number of the EIS data, the coating impedance variation trend in low frequency range has a corresponding impedance variation trend in high frequency range. Based on this idea, this work introduces an EIS-based sensor system designed for coating performance evaluation. The sensor system consists of one base station and one sensor node. Wireless communication is realized between the sensor node and the base station. The sensor node is smaller than a business card in size. Evaluation time is less than 10 seconds in the operation frequency range between 20 - 90 kHz. Three coated panels were used for testing. Testing results are presented for both the EIS instrument and the sensor system. Good correlations indicate that this new technique is valid for EIS based coating performance evaluation in high frequency range. The sensor system is powered by batteries. The power consumption is 420 mW which is lower than the commercial EIS instrument. The sensor system is portable and easy to use in real time for field coating performance evaluation.

ACKNOWLEDGMENTS

TABLE OF CONTENTS

LIST OF TABLES

LIST OF FIGURES

CHAPTER 1. INTRODUCTION

Metal corrosion is a costly problem in business and industries throughout the world. Only in the aircraft industry, billions of dollars are lost due to the corrosion of metal every year [1]. In addition to the business cost, many mechanical failures are caused by corrosion. One example is the Aloha Airlines 737, which lost the upper half of the fuselage during the flight at 24, 000 feet in the air because of the metal corrosion of the aircraft. Beyond the business cost issues, corrosion threatens the public safety as well. Traditionally, coating is a major approach for surface protection of a structure. Coatings play an important role in the industries and our real life. Because of the need for reducing maintenance cost and tackling public safety issues, research works on coating evaluation for preventing corrosion become more and more important.

Generally, coating is treated as a barrier for metal structures, reducing the transport of water, ions, and oxygen from the environment to the metal substrate [2]. Most of the time, corrosion begins as moisture penetrates the protective barrier of a structure, such as coating, beginning an electrochemical process which leads to surface crack and pitting. The pitted or cracked surface of a structure can cause advanced damage, such as through-thickness crack, fracture, deformation, etc., while encountering mechanical stress. These structural damages are potential safety threats. On reducing the business cost and tackling safety issues, researchers worked on detecting, controlling, and preventing corrosion over the past few decades [9, 12, 22].

Coating evaluation by providing feedback information about the protection performance of the coatings can monitor whether coatings operate at their most healthy status. Coating evaluation greatly increases the safety of the structures under the protective coatings. Traditionally, two major coating evaluation methods, namely Electrochemical Noise Method (ENM) and EIS, are used. The ENM

technique measures the electric potential noise and current noise fluctuations which originate from the coating samples. Because no outside perturbation is required, the ENM coating evaluation technique is a non-intrusive and Non-destructive Evaluation (NDE) technique. Using ENM for corrosion process study and coating performance evaluation was first reported in the late 1960s and 1970s [16,29]. Innovative research works on coating evaluation using ENM in the past few years have been presented in published papers [6,17,23]. Different from ENM technique which measures the electric noise fluctuations originated from the coating sample, EIS measures the impedance and phase variation under a typical 0.01 Hz to 100 kHz frequency sweep [7]. After EIS was first introduced in the time frame of 1880 to 1900 by Oliver Heaviside [18], EIS has established as a powerful tool for investigating coating protective properties and studying corrosion process by researchers. Compared to the ENM technique, EIS is more widely used in the past 25 years. EIS studies and applications, such as corrosion process study, coating performance evaluation, have been presented in published papers [13,14]. Since the amplitude of the outside supplied perturbation is very small (0.01 mV to 0.5 mV), EIS measurement is a NDE technique as well as ENM. ENM and EIS are two major tools for coating study and evaluation. ENM is more useful for identifying corrosion type and locating corrosion place while EIS is more useful on coating remaining life prediction as reported in the published papers [7,28].

There are other advanced methods for coating evaluation and corrosion control study. In 2000, Fu et al. proposed a method for studying coating failure and coating evaluation using acoustic emission [10]. Sekin et al. used the electrochemical, physio-chemical and physical measurements to study the degradation of the coating corrosion protective properties in 2002 [25]. In 2005, Simmers presented a method using beams to detect corrosion and study corrosion damage in quantification. Coating corrosion resistance evaluation using lead zirconate titnate sensors was also introduced by

Simmers in his work [27]. However, these works as well as traditional EIS and ENM techniques requires bulky equipment and expensive anlyzers. For example, $PC4^{TM}$, a widely used EIS analyzer produced by Gamry Instruments, Inc, cost nearly $4000. In addition, the bulky equipment and complicated electrode connection required by traditional EIS technique is not conducive to do real time coating evaluation in the field.

This work aims to introduce a low cost, low power consumption, EIS-based sensor system designed for coating performance evaluation. The sensor system consists of a sensor node and a base station. Based on the idea of measuring coating impedance in a frequency range, the sensor node generates its own variable frequency sweep and applies to the coating. The impedance response can be obtained and processed by the sensor node. The sensor node sends impedance data to the base station through wireless communication. This realizes long distance remote coating evaluation in the field.

CHAPTER 2. THEORETICAL BACKGROUND

2.1. EIS Coating Evaluation

EIS measures the coating impedance and phase in a frequency range. The coating impedance indicates the coating corrosion resistance performance while the coating phase information indicates the coating damage type and coating remaining life prediction [5].

In EIS coating evaluation, the coating sample is generally immersed in the electrolyte solution. Figure 1 shows a typical coating model for EIS analysis. In figure 1, R_{sol} is the solution resistance; C_{sol} is the solution capacitance; C_{coat} is the coating capacitance; R_{pore} is the pore resistance; R_{PR} is the polarization resistance; C_{DL} is the double layer capacitance. When coating is damaged or degraded, the resistance and the capacitance will change. Changes in the coating capacitive components reflect the coating phase variations. The resistive component change indicates coating corrosion resistance property [21]. The EIS-based coating phase measurement is not included in this work.
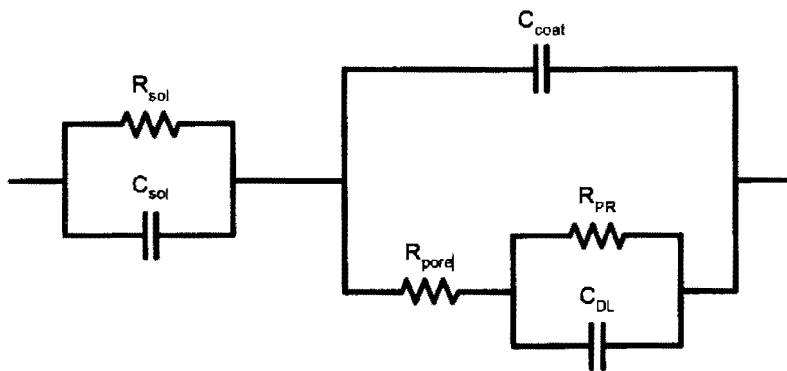
Figure 1. A typical coating model used for EIS analysis [21]

Since the coating impedance under a frequency range reflects coating corrosion resistance property [11], protection performance of coatings can be evaluated by

measuring coating impedance in a frequency range. Traditional frequency range used for EIS is from 0.1 Hz to 100 kHz. EIS evaluates the coating impedance value at very low frequency. From the EIS point of view, generally, coating with the impedance greater than 10^9 Ω/cm^2 at 0.1 Hz can be considered to provide excellent corrosion resistance performance, while those possessing impedance lower than 10^6 Ω/cm^2 at 0.1 Hz are said to be a poor state in corrosion resistance [20]. Coating impedance measurement at 0.1 Hz can easily distinguish different coating performance but requires long measuring time (longer than 15 minutes) [11].

2.2. EIS-based Coating Evaluation by the Proposed Sensor System

2.2.1. Theory

After observing a large number of EIS data on different coatings, the correlation between coating impedance variation trend at single low frequency and frequency-impedance (f-i) curve variation trend in high frequency was found. In other words, the impedance at low frequency (lower than 1 Hz) has a corresponding section of f-i curve in high frequency range (higher than 20 kHz). Most of the time, the f-i curve at high frequency range has the same impedance variation trend as the coating impedance in low frequency.

Figure 2 shows the relation between coating impedance at low frequency and f-i curve in high frequency range. The tested coating sample is measured by EIS for 22 days. The frequency versus impedance plot is presented. In low frequency range (0.01 Hz to 1 Hz), the coating impedance is decreased from Day 1 to Day 22. The zoom in EIS data view in high frequency range is illustrated in the upper-right corner of the figure. The same variation trend was observed for f-i curve in high frequency range.

Therefore, f-i curve in high frequency also can be used for corrosion resistance performance of a coating. Different from the EIS traditional single low frequency
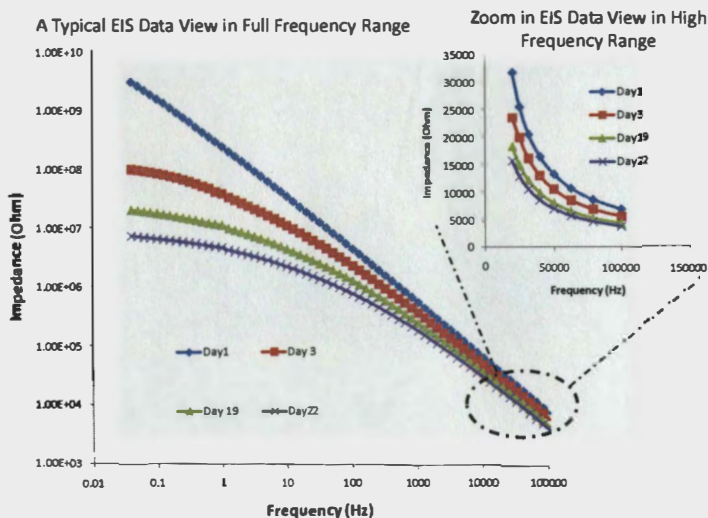
Figure 2. Illustration of the relation between coating impedance in low frequency and f-i curve in high frequency

coating impedance quantitative analysis, f-i curve variation in high frequency range is studied qualitatively.

Coating corrosion resistance examination at low frequency requires very long measurement time. In addition, bulky equipment and expensive electrode connection by EIS is needed for accurate low frequency coating impedance measurement [2]. This is not conducive for real time coating degradation evaluation in the field.

2.2.2. Coating Measurement Model

Based on the idea of measuring coating f-i curve in a high frequency range, a coating measurement mode is presented in this section. In figure 1, the coating is modeled as a combination of resistors and capacitors. Changes in the coatings results in the changes of the resistive components and the capacitive components. The overall coating impedance is thereby changed. The proposed EIS-based sensor system measures the overall equivalent impedance of the coating.

Figure 3 shows a simplified model of the coating impedance measurement. A coating sample is immersed in an accelerated coating degradation environment. The
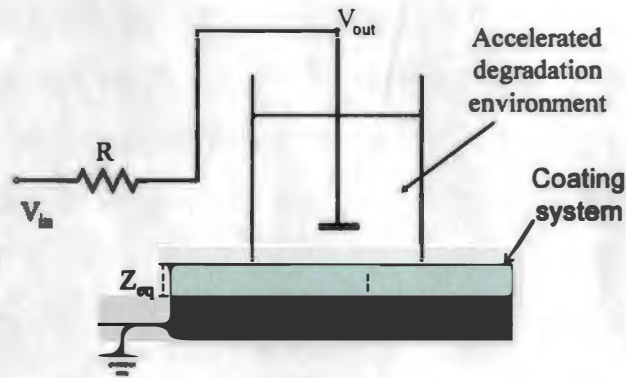
Figure 3. Simplified model of coating measurement

frequency sweep with amplitude voltage (V_{in}) is applied to the coating through a resistor R. The peak voltage and wave shape after the resistor will change due to the complex electronic model of the coating. According to the voltage division theory, the overall equivalent coating impedance can be obtained by measuring the peak voltage variation at V_{out}. The equivalent coating impedance (Z_{eq}) can be calculated by the known peak voltage (V_{in}), the known resistor value R and the measured output voltage (V_{out}). Because of capacitive components in the coating, different frequencies will result different equivalent coating impedance (Z_{eq}). The following equation shows the impedance calculation. The resistance value of the resistor (R) in this work can be adjusted to meet different coatings with different impedance.

$$\frac{V_{in} - V_{out}}{R} = \frac{V_{out}}{Z_{eq}} \tag{1}$$

The frequency range used in this work is 20 kHz to 90 kHz. The peak voltage V_{in} used in this work is 4.8 V. Although EIS analysis uses small amplitude voltage, coating degradation is not accelerated by the selected V_{in} since the coating is examined under a high frequency and the examination process only lasts few seconds [3]. Unlike the low frequency impedance variation, which is usually several orders in magnitude, the high frequency impedance change is much smaller. Based on the relation between

7

f-i curve in high frequency and impedance in low frequency, the high frequency impedance change still can be used for distinguishing different coating performances by the proposed simple cost-effective sensor system.

Coating performance can be qualitatively evaluated by analyzing f-i curve variation in a higher frequency range. The experiments in this work demonstrated the feasibility of this idea (introduced in Chapter 4).

CHAPTER 3. DESIGN AND OPERATION OF THE EIS-BASED SENSOR SYSTEM

The design and operation of the proposed EIS-based sensor system is presented in this chapter.

The proposed sensor system consists of one sensor node and one base station. The sensor node contains a Frequency Sweep Generator (FSG), a frequency multiplier, an peak detector, a Analog to Digital Converter (ADC), a control unit and a wireless transmitter. The base station contains a wireless receiver, a microcontroller and a RS232 as the interface between the base station and the PC. Both the sensor node and the base station are powered by four AAA 1.5 V batteries. Figure 4 shows the block diagram of the proposed sensor system.
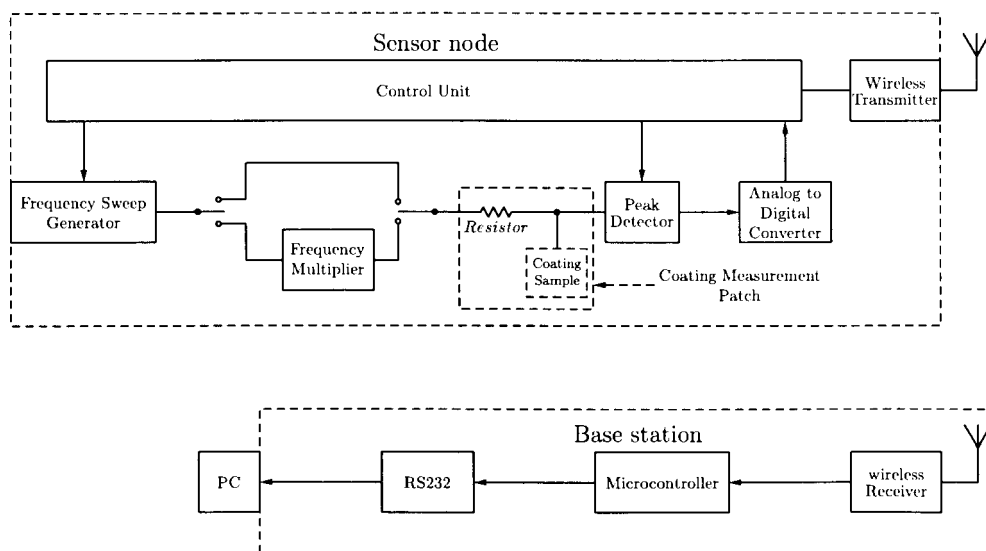
Figure 4. Block diagram of the proposed sensor system

As shown in figure 4, the sensor node is attached to a coating sample. The sensor node measures the coating impedance. Once the sensor node obtains the impedance data, the sensor node sends the data to the base station through wireless communication. The base station processes the data, then sends the data to a PC.

9

The wireless communication used in this work is one way wireless communication. In other words, the base station only receives data from the sensor node.

3.1. Description of the Sensor Node Design

The proposed EIS-based sensor node is realized on the Printed Circuit Board (PCB). The sensor node has functions of frequency sweep generation, voltage peak detection, analog to digital data conversion and operation control. The frequency sweep generation, analog to digital conversion and operation control functions are realized by using a microcontroller (PIC16F876, Microchip, Inc). Because a smaller sensor node is easier to realize coating evaluation in field, reducing the prototype size of the sensor node is considered in the sensor node design. Since a microcontroller can perform functions such as an analog to digital converter (ADC), timing control, data flow control and interface with other circuits and systems, the prototype size of the sensor node can be greatly reduced [26, 27] by using microcontroller in the sensor node design. The sensor node is less than a business card in size as shown in figure 5.

Figure 5. Actual size of the sensor node

3.1.1. FSG

The FSG is used to generate a square wave within a certain frequency range. In this work, the FSG generates a square wave frequency in a range of 20 kHz to 90 kHz in the consideration of time efficiency and reliable signal. The FSG design is based on the internal timer of the microcontroller. PIC16F876 has 3 internal timers: timer 0, timer 1, and timer 2 [26]. Timer 1 is selected and used in a compare model to build FSG in this work. Timer 1 can drive an I/O pin high or low at precisely controlled time.

A 20 MHz crystal oscillator is selected as the input frequency of the microcontroller. According to the data sheet of PIC16F876, the input frequency for the timer 1 compare mode is

$$f_{timer1} = \frac{f_{OSC}}{4} = 5MHz \tag{2}$$

The microcontroller interrupts after timer 1 counts to a certain event. When each interrupt is trigged, a square wave with a fixed frequency can be obtained by toggling an I/O pin. The variable frequency can be obtained by changing the events that timer 1 needs to count. Equation 3 shows the relation between the generated frequency and the counted events for interrupt.

$$f_{FSG} = \frac{5,000,000}{2 \times N} \tag{3}$$

f_{FSG} is the output frequency of the FSG. N is the event needs to count for interrupt requests. For instance, a 30 kHz frequency can be obtained by setting N is equal to 83. A continuous changing event N results in a continuous changing frequency f_{FSG}.

The frequency range generated by FSG is 38 Hz to 50 KHz in this work. Wider

11

frequency range can be obtained by using a frequency multiplier.

3.1.2. Frequency Multiplier

A frequency multiplier is designed for a wider frequency sweep range. With the frequency multiplier, the sensor node can generate multiple frequency ranges. The frequency multiplier contains a Phase Lock Loop (PLL) (CD4046B) and a clock divider (74ls92).

CD4046B is a commercial PLL device. The PLL can function as a frequency multiplier by inserting a clock divider into the feedback loop between the Voltage Controlled Oscillator (VCO) output and the phase comparator input [15].

Figure 6 illustrates the frequency multiplier design. The error voltage at the output of the phase comparator $V_{e(t)}$ is zero if there is no input signal. The voltage at the output of the Low Pass Filter (LPF) is also zero. The Voltage Controlled Oscillator (VCO) thereby operates at a free running frequency, f_{free}. When an input frequency is applied to the phase comparator, the phase comparator compares the phase and frequency of the input signal with the VCO frequency then generates an error voltage. The error voltage is filtered by the LPF and applied to the input of the VCO. The error voltage, $V_{e(t)}$, is proportional to the phase differences. $V_{d(t)}$ is the output voltage of the LPF.
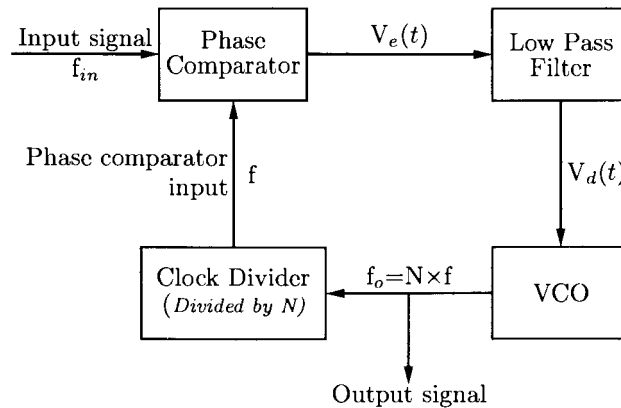
Figure 6. Block diagram of frequency multiplier design

The VCO output frequency is proportional to the input voltage $V_{d(t)}$ as shown in figure 7. Figure 7(a) shows frequency versus voltage without offset. Figure 7(b) shows frequency versus voltage with offset. $V_{d(t)}$ varies in a direction that reduces the phase and frequency differences between the VCO and the input signal. $V_{d(t)}$ adjusts the frequency differences between the input signal and the VCO frequency. When the frequency generated by the VCO is sufficiently close to the input frequency, the entire loop is in a lock state. The phase comparator input f is equal to the input frequency f_{in}. A clock divider is added between the VCO frequency output and the frequency input of the phase comparator. The clock divider divides input frequency by N (N=2, 4, 8, 12) based on different configuration of the 74ls92 [8].

(a)   (b)
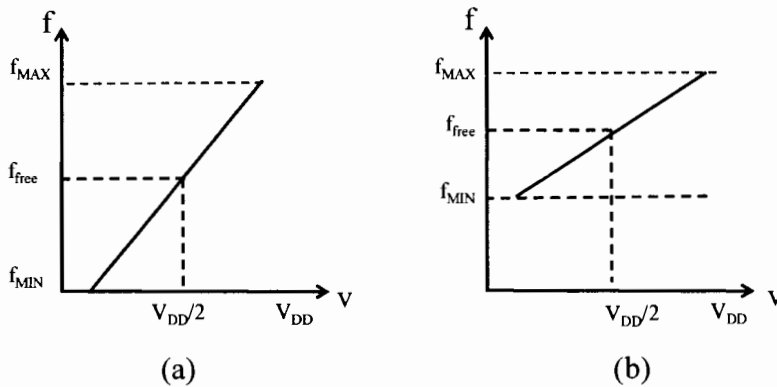
Figure 7. Plot of VCO output frequency versus input voltage

Figure 8 shows the pin connection of the frequency multiplier. In figure 8, the Pin 12 of CD4046B is not connected because the resistance at Pin 12 has to be infinity in order to obtain a no-offset VCO setup. Pins 6, 7, 11 connection configures the free running frequency of the VCO. The clock divider is configured as divided by 12.

3.1.3. Peak Detector

The frequency sweep from the frequency multiplier is applied to the tested coating sample through a resistor. A peak detector is needed to track and hold the amplitude value of the signal from the tested coating sample. Figure 9 shows the
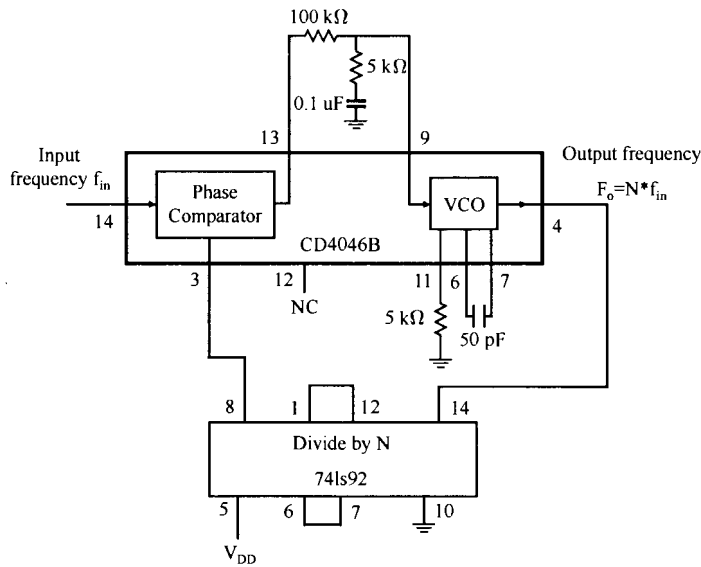
Figure 8. Pin connection of the frequency multiplier

diagram of the peak detector.
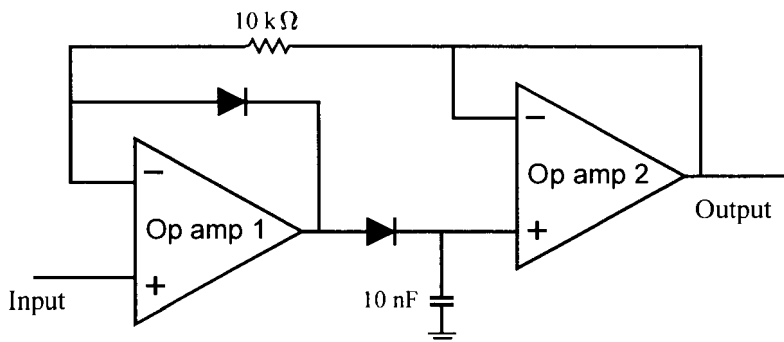
Figure 9. Diagram of the peak detector

The peak detector is simulated by the PSPICE. Figure 10 shows the simulation result. As shown in figure 10, the output signal (dashed line) tracks and holds the peak voltage value of the input signal until the next peak arrives.

MCP602 is selected for the peak detector design in this work. MCP602 contains two single power supply op amps. The single power supply op amp was selected to

14
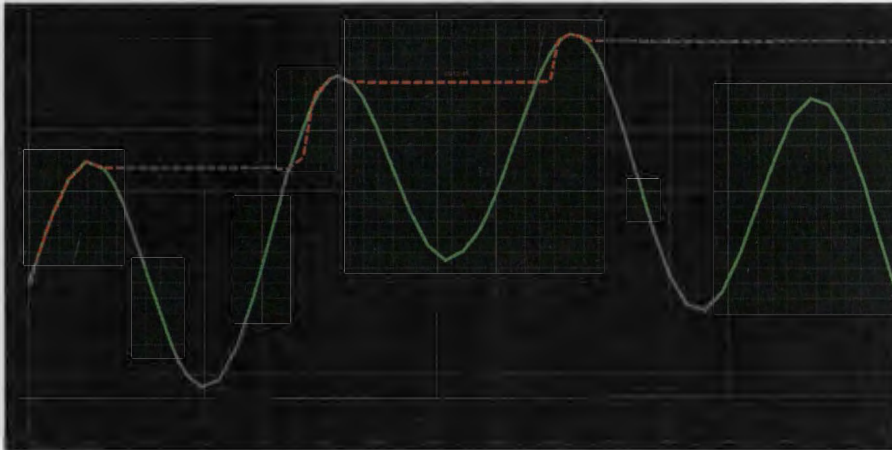
Figure 10. Simulation result of the peak detector

meet the battery power supply requirement. Since the 8-pin MCP602 has two op amps, the sensor node size can be reduced. Figure 11 shows the pin connection of the peak detector.
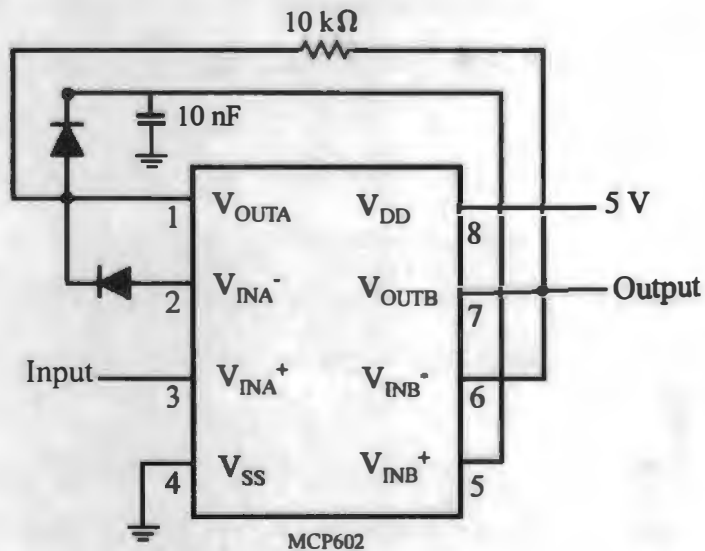
Figure 11. Pin connection of the peak detector

3.1.4. ADC

The ADC is designed for converting the analog voltage value captured by the peak detector to the digital value. The ADC design in this work is based on the

15

PIC16F876 application. The PIC16F876 has an internal 10-bit ADC module [26]. The A/D conversion of the analog input signal results in a corresponding 10-bit digital number.

The ADC module has four registers. They are: ADC Result High Register (ADRESH), ADC Result Low Register (ADRESL), ADC Control Register 0 (AD-CON0) and A/D Control Register 1 (ADCON1). The ADCON0 register controls the operation of the ADC module. The ADCON1 register configures the function of the port pins which include ADC input selection and reference voltage source selection. The ADRESH:ADRESL registers contain the 10-bit converted result of the analog to digital conversion. When the conversion is complete, the result is loaded into this A/D result register pair.

Figure 12 shows the ADC block diagram. the RE0–RE2 pins shown in figure 12 is not available in the PIC16F876. The analog input can be selected by CHS2:CHS0 combinations. For the reference voltage, V_{DD} (5 volts) is selected for V_{REF+} and V_{SS} (0 volt) is selected for V_{REF-}.

The acquisition time T_{ACQ} for the ADC module in PIC16F876 includes ampli-fier settling time (T_{AST}), hod capacitor charging time (T_{HC}) and the temperature coefficient (T_{TC}) [26]. According to the PIC16F876 datasheet, T_{HC} is given as 16.47 μs. The following equation shows the acquisition time calculation.

$$T_{ACQ} = T_{AST} + T_{HC} + T_{TC} \tag{4}$$

$$= 2\mu s + 16.47\mu s + [(Temperature - 25^oC) \times (0.05\mu s/^oC)] \tag{5}$$

$$= 2\mu s + 16.47\mu s + [(50^oC - 25^oC) \times (0.05\mu s/^oC)] \tag{6}$$

$$= 19.72\mu s \tag{7}$$

Consequently, the sampling rate of the ADC used in this work is given in
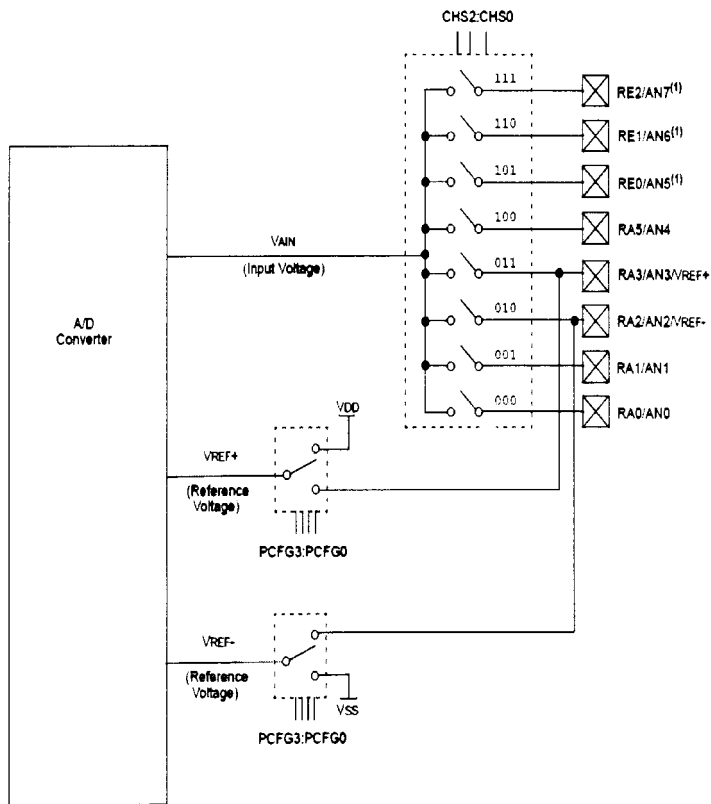
Figure 12. Block diagram of the ADC module [26]

equation 8.

$$f_{sample} = \frac{1}{T_{ACQ}} = 50.71 kHz \tag{8}$$

This sampling rate is fast enough since the ADC only converts the DC voltage value from the peak detector.

In this work, the V_{REF+} uses 5 volts and V_{REF-} uses 0 volt. The allowed maximum input analog voltage is 5 volts. Therefore, the resolution of the ADC is:

$$\frac{5V}{2^{10}} = 4.88mV \tag{9}$$

Suppose the converted digital value is $N_{digital}$, the following shows the ADC conversion.

$$\frac{5V}{2^{10}} = \frac{V}{N_{digital}} \tag{10}$$

Hence, the corresponding ADC input voltage V is shown in equation 11.

$$V = 4.88mV \times N_{digital} \tag{11}$$

After the analog to digital conversion, the ADC sends the digital number, $N_{digital}$, to the control unit.

3.1.5. Control Unit

The control unit controls the sensor node operation. The control unit adjusts the frequency generation of the FSG, resets the peak detector (discharge the hold capacitor in peak detector), collects data from ADC and sends data to the wireless transmitter.

PIC16F876 has three I/O ports. Timing control and I/O port operation are

major approaches to operates the sensor node. The control unit controls the FSG. When the FSG receives the request from the control unit, it starts to generate a square wave with a fixed frequency. The control unit determines whether the frequency multiplier is required or not. Then the control unit connects or disconnects the frequency multiplier from the FSG based on different situations. The peak detector and the ADC obtains and converts the data. The control unit collects the data from the ADC. The control unit will further process the data then sends to the wireless transmitter for data transmission. After the wireless transmitter sends the data out, the control unit reset the peak detector then sends a increase frequency request to FSG. The FSG increases the frequency, then the measurement cycle is repeated. After the coating sample is measured in the full frequency sweep, the control unit reset the FSG, peak detector and the ADC. The control unit runs the sensor node in a sleep mode to save power.

In this work, PORTA is used for analog signal control, such as ADC reference voltage selection, ADC input pin selection. PORTC is used for I/O control and timing control. RC4 in the PORTC is used for frequency sweep generation by the FSG. PORTB connects with Light-emitting diodes (LEDs) for sensor node status checking purpose.

3.2. Description of the Base Station

The base station receives data from the sensor node then sends data to a PC through Serial Communication Interface (SCI). The base station contains a wireless receiver and an interface between the PC and the base station. The wireless receiver design is introduced in Section 3.3.

3.2.1. Serial Communication Interface Design

The Universal Asynchronous Receiver Transmitter (UART) module is used to build the SCI for communication between base station and the PC. Pins RC6 and

RC7 in PORTC can be worked as a transmitter (TX) and a receiver (RX) if proper values are written to the register. In order to make RC6 and RC7 work as universal asynchronous receiver transmitter, the RC6 and RC7 value has to be set to high, and the Single Receive Enable bit (SPEN) bit in the Receiver Status and Control Register (RCSTA) must be set to 1 to enable the serial port in the PIC16F876. The Transmit Status and Control Register (TXSTA) controls the clock source selection and the baud rate settings.

According to the PIC16F876 datasheet, the data is sent and received as a start bit (high to low transition), 8 data bits and 0 to 2 stop bits. Since there is no clock for data communication between the PC and the base station, the PC and the base station must know how long each bit it is. Setting the same baud rate can address this issue.

The high baud rate select bit (BRGH) in the TXSTA register controls the baud rate speed selection. The high speed mode requires the BRGH set as 1 while the low speed mode requires the BRGH is set equal to 0. Equation 12 and 13 shows the baud rate formula in high speed mode and in low speed mode, respectively.

$$BaudRate = \frac{F_{OSC}}{16 \times (X+1)} \tag{12}$$

$$BaudRate = \frac{F_{OSC}}{4 \times (X+1)} \tag{13}$$

X is the Baud Rate Generator Register (SPBRG) value. In this work, the 115 kbps baud rate is selected for the PC and the base station. The oscillator frequency used for the microcontroller is 20 MHz. The low speed baud rate mode is selected (BRGH=0). Based on Equation 13, X value is:

$$X = \frac{F_{OSC}}{16 \times BaudRate} - 1 \tag{14}$$

$$= \frac{20 \times 10^6}{16 \times 115 \times 10^3} - 1 \tag{15}$$

$$= 10 \tag{16}$$

Therefore, settings of SPBRG=10, BRGH=0, SYNC=0 and BRG16=1 are required for obtaining a 115 kbps baud rate.

Figure 13 shows the hardware connection for SCI communication from the base station to the PC. MAX232A is selected for UART module.
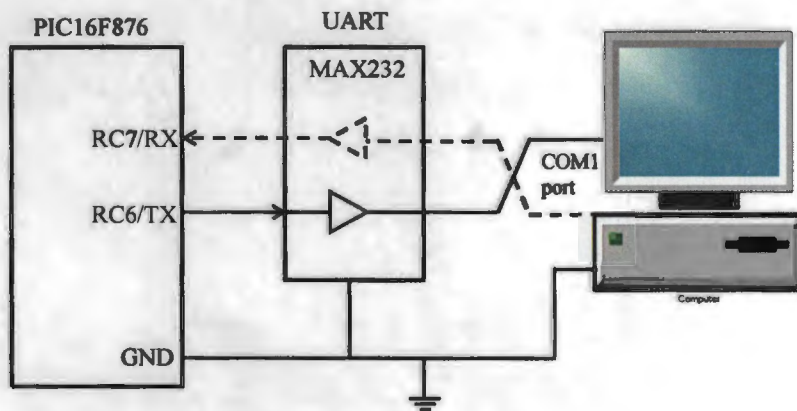
Figure 13. Hardware connection for SCI communication

3.3. Wireless Communication

Wireless communication is realized in this work for real-time remote coating evaluation purpose. An HP series transmitter, TXM-900-HP3-PPO, and an HP series receiver RXM-900-HP3-PPO (Linx technologies, Inc) is used in this work to realize wireless communication. The reason for selecting this transceiver is that the HP series transceiver usable range is up to 1,000 feet. It also provides 8 parallel, 100 serial

user-selectable channels. These features make long distance, multi-location coating evaluation possible in the future work. The HP series transceiver also has power down feature which can be used for power saving purposes. The wireless transmitter and wireless receiver are controlled by the PIC16F876.

Figure 14 shows the pin diagram of the wireless transmitter. ANT (pin 2) is the 50 Ω RF output. Pin 2 is connected to an antenna with matched impedance. CS0, CS1 and CS2 (pin 3 to pin 5) are the channel selection ports. Different combinations of CS0, CS1, and CS2 determine different signal carrier frequencies. Pin 7 PDN controls the power down feature. Pulling this line low will place the transmitter into a low-current state. The module will not be able to transmit a signal in this state but will run in a low power consumption model. Mode (pin 9) is the mode Selection. Setting pin 9 as GND is for parallel channel selection and setting pin 9 as VCC is for serial channel selection. Pin 10 is the data input pin.
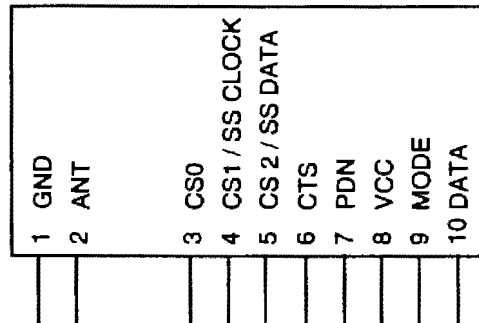
Figure 14. Wireless transmitter pin map

When the data is sent to the transmitter through data input, the transmitter modulates the data. The frequency of the carrier signal is determined by the channel selection port (CS0:CS3). The modulated signal is sent to RF output for wireless communication.

Figure 15 shows the pin diagram of the wireless receiver. Most of the pins of the wireless receiver are the same as the pins of the transmitter. Pin 14, RSII, is

22
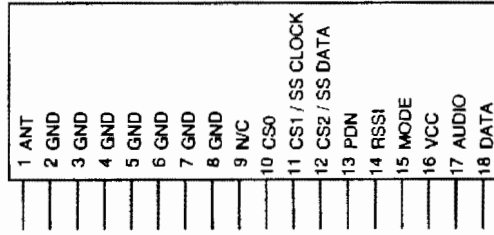
Figure 15. Wireless receiver pin map

the received signal strength indicator. This line will supply an analog voltage that is proportional to the strength of the received signal. The AUDIO pin at pin 17 is the recovered analog output. The DATA pin at pin 18 is the digital data output. This line outputs the demodulated digital signal. The coating impedance data is communicated as digital data in this work. Therefore, the DATA pin is selected.

When the wireless receiver receives data from the RF input (ANT pin), the wireless receiver will demodulate the signal and send the demodulated data out through the DATA pin.

In the sensor node, RC0, RC1 and RC2 in the I/O PORTC controls the status of the channel selection port. RC3 controls the PDN status. RC5 connects to MODE pin. DATA pin is connected to the RA5 in the I/O PORTA. In the base station, the same configuration is required for channel selection port control. RSSI pin is connected to a LED to indicate the signal strength.

Between the sensor node and the base station, data are sent as 4 start bits, 10 data bits and 0 stop bit. The wireless receiver in the base station keeps listening the incoming data package. Once a data package is detected, the base station firstly checks the start bits. Only the right start bits allow the base station to collect the data. After that, the base station checks the data integrity. Only the valid data is sent to PC for further data processing.

During the wireless communication, only if the matched channel is selected, the transmitter and the receiver can communicate with each other. Therefore, the same

23

setting for CS0:CS1 is required. Table 1 shows the parallel channel selection. The channel selection feature can realize the multi location remote coating evaluation in field.

Table 1. Parallel channel selection table

CS2	CS1	CS0	Channel	Frequency (MHz)
0	0	0	1	903.37
0	0	1	2	906.37
0	1	0	3	907.87
0	1	1	4	909.37
1	0	0	5	912.37
1	0	1	6	915.37
1	1	0	7	919.87
1	1	1	8	921.37

After the base station receives the coating impedance data from the sensor node, it will send the data to the PC for further processing through SCI communication.

3.4. Sensor System Operation for EIS-based Coating Evaluation

In this section, the detailed description of the sensor system operation is presented.

The task of the sensor node is to generate frequency sweep and to apply to the coating, then to record the impedance and frequency information. After collecting the required data, the sensor node sends the data to the wireless transmitter for communication. The task of the base station is to listen and receive the data package from the sensor node. Once the base station receives the data, it will send the data to the PC only if the data is valid.

In the hardware design of the sensor node, a switch is placed and connected to the microcontroller to generate a start a task signal. Another switch is placed to generate a signal for frequency selection. When power is on, the control unit in the sensor node starts to wait for the start-a-task signal. In the meantime, the control

unit connects the FSG to frequency multiplier or bypass the frequency multiplier based on the frequency multiplier selection signal. Once the control unit receives the start-a-task signal, it will send a begin signal to the FSG. The FSG then starts to generate an initial frequency. In this work, the FSG can not generate the full frequency range required by the proposed EIS-based coating evaluation. In this case, the initial frequency from the FSG is amplified by the frequency multiplier and applies to the coating sample through a resistor. Because of the complex model of the coating sample and the voltage division theory, the wave shape after the resistor is changed. The peak detector tracks and holds the amplitude voltage of the signal between the resistor and the coating sample. The peak detector sends the DC voltage to the ADC. The ADC sends a AD conversion start signal to the control unit before starting a AD conversion. Once the control unit receives the AD conversion start signal, it will change the PDN of the wireless transmitter from low to high to enable the wireless transmitter. After the ADC converts the analog DC voltage to a digital number, the ADC sends the digital DATA to the control unit. The control unit then sends both the impedance data and frequency data to the wireless transmitter. When the wireless transmitter receives the data, it will firstly modulate the data, then sends the data to the base station through wireless communication. After sending the data to the wireless transmitter, the control unit resets the peak detector and the ADC, then the control unit sends a request to the FSG to increase the frequency to the next step. The control unit will run the wireless transmitter in a low current state until the ADC completes the next data conversion. The measurement cycle is repeated until the impedance measurement is complete at the last frequency. When the entire coating impedance measurement cycle is completed, the control unit will reset all the devices and run the sensor node into a low power consumption state.

During the whole measurement cycle of the sensor node, the base station keeps

25

listening the incoming data package of each single measurement cycle. The wireless receiver in the base station demodulate the signal from the wireless transmitter, then sends to the PIC16F876 in the base station. After getting the correct data. the base station sends the impedance and frequency data to the PC for further data processing.

According to the real case measurement, the amplitude voltage applied to the resistor before the coating is 4.8 volts. The impedance data that the PC received is the converted digital number. Combining equation 1 and equation 11, the PC calculates the coating impedance data in ohms. Equation 17 shows the final coating impedance calculation. The PC plots the f-i curve based on the impedance and frequency data received by the sensor system.

$$Z_{final} = \frac{4.88mV \times N_{digital} \times R}{4.8V - 4.88mV \times N_{digital}} \tag{17}$$

R is the resistor value before the coating. Resistance R can be adjusted to evaluate different coatings with different impedance.

CHAPTER 4. EXPERIMENT

Three coating performance evaluation experiments were conducted to verify the feasibility of the proposed sensor system. The coating system used in this experiment includes one component coating system (primer) and two components coating system (primer and topcoat). Three coating samples were tested by the proposed sensor system: the two components Epoxy-Polyamide primer and Akzo Nobel Aerospace Coating (ANAC) topcoat, one component Magnesium(Mg)-Rich Primer, and two components Mg-rich Primer and ANAC topcoat. These coating samples were tested by the EIS commercial instrument as well for the data comparison purpose. Since the systematic error caused by the hardware in the sensor node, calibration is required for data processing. After calibration, similar experimental results were obtained by the EIS Instrument and the sensor system which demonstrate the feasibility of the proposed sensor system.

4.1. Experiment Design

Three coating samples were immersed in the electrolyte solution for accelerated coating degradation purposes. In order to prove the proposed sensor system can properly conduct EIS-based coating evaluation, coating samples were also tested by the commercial EIS instrument. In this section, the coating sample preparation, experimental setup for EIS instrument and sensor system are presented.

4.1.1. Coating Sample Preparation

The coating samples used in this work were prepared based on the methods of the previous research work on coating sample preparation [24]. Aluminum (Al) alloy 2024-T3 panels, supplied by Q-panel Lab Products of Cleveland OH, were first pretreated in phosphate alcohol solution for 4 minutes. The panels were then rinsed with tap water until a water break free surface of the panel is obtained. Then the

panels were rinsed again with deionized water, and lastly the panels were dried with dry nitrogen flux. The panels were used in the experiments within 3 days after they had been pretreated.

Different organic coatings were applied to the pretreated AA 2024-T3 panels using a regular air spray gun according to the standard application procedures provided by the coating manufacturer. After the fresh coating had been air dried for 7 days, their thicknesse values were measured with an Elcometer and ready for the testing. Table 2 shows the coating thickness of the samples used in this work.

Table 2. Thickness of the coating samples

Coating System	Primer Thickness (μm)	Total Thickness
Epoxy + ANAC	25+50	75±5.
Mg-rich	50	50±3
Mg-rich +ANAC	50+50	100±6

Before the coating samples were tested, a cell with 8 cm^2 area was placed on top of the coating sample. The electrolyte solution was filled in the cell. The electrolyte solution used in this work was Dilute Harrison's Solution (DHS), which contains 0.05% NaCl and 0.35% $(NH_4)_2SO_4$, and the exposing area is about 8 cm^2. The DHS is used for accelerated coating degradation purpose in this work.

Figures 16, 17 and 18 show the three coating samples used in this work.

Figure 16. Epoxy primer with ANAC topcoat coating sample

4.1.2. EIS Coating Evaluation Setup

Figure 17. Mg-rich primer coating sample

Figure 18. Mg-rich primer with ANAC topcoat coating sample

A PC4^{TM} instrument from Gamry Instrument, Inc was used for EIS evaluation on coating samples.

EIS coating evaluation is performed by using three electrodes and an electrochemical cell. The three electrodes used by EIS are: counter electrode, reference electrode and working electrode. The reference electrode is a saturated calomel electrode. The counter electrode is connected to a platinum mesh electrode. Al substrate of the coating sample is connected to the working electrode [19]. The EIS instrumentation consists of a PC-4 potentiostat coupled to an eight-channel multiplexer which is controlled by CMS100/300 software (Gamry Instrument).

Figure 19 shows the EIS electrodes connection for coating evaluation. Figure 20 shows a picture of the electrodes connection on a coating sample. As shown in figure 19, the coating sample is exposed to the DHS for accelerated coating degradation. The counter electrode and the working electrode generates a perturbation with an amplitude voltage V and applied to the coating. The counter electrode and the working electrode also measures the output current I. The coating impedance can be calculated based on the Ohm's law. The reference electrode functions as system calibration.

4.1.3. Sensor System Coating Evaluation Setup

Figure 21 shows the sensor system coating evaluation setup. The sensor node attaches to a coating sample and measures the coating impedance. The sensor node processes the data and sends the data to the base station through wireless communication. The base station receives data and sends the data to a PC through SCI communication. Both of the sensor node and the base station are powered by four 1.5 V AAA batteries.

The coating sample was exposed to DHS which is the same as the EIS setup. The sensor node has two electrodes: a substrate electrode and a working electrode.
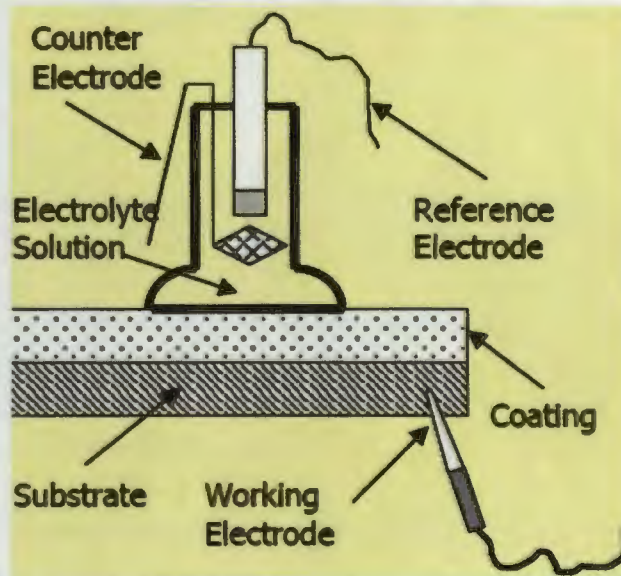
30

Figure 19. EIS electrodes connection for coating evaluation

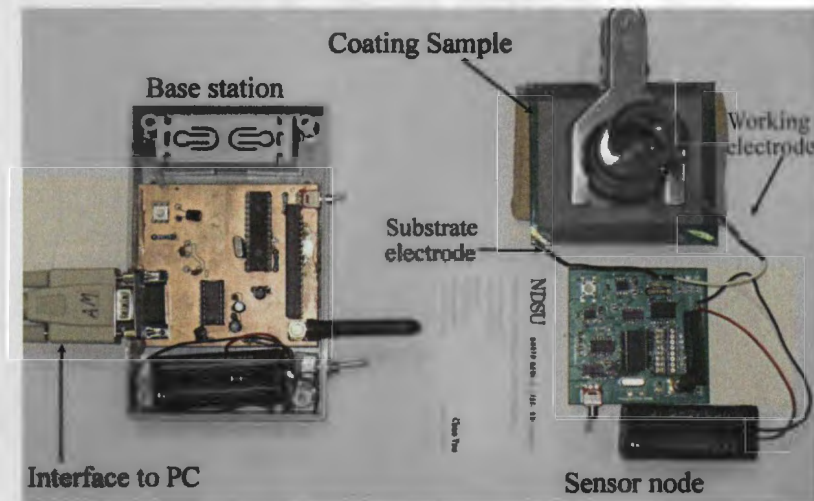Figure 20. Real picture of the EIS electrodes connection

Figure 21. Sensor system setup for EIS-based coating evaluation

As shown in figure 21, the substrate electrode is connected to the Al substrate, the working electrode is connected to a platinum mesh electrode. The platinum mesh electrode is immersed into the DHS. The impedance between the substrate electrode and the working electrode obtained by the sensor node is the approximately impedance of the coating system on Al panel. Coating impedance in a frequency range will change depending on the degradation of the coating performance. In other words, the electrodes between the DHS and the substrate can detect the impedance variation a coating sample.

4.2. Experiment Results

Experimental results for the three tested coating samples are presented in this section. Results obtained by the EIS instrument and results obtained by the sensor system are compared.

4.2.1. Epoxy Primer + ANAC topcoat

The coating system used in this experiment comprises of an Epoxy primer beneath an ANAC topcoat. The coating system was applied to an Al plate (5×5×0.2 cm³). The coating sample was tested by both the proposed sensor system and the

EIS instrument. The f-i curve plotted by the sensor system and EIS instrument are compared.

The f-i curve plot in terms of immersion time by the sensor system is shown in figure 22. Impedance of the coating sample was measured with frequencies of 25 kHz, 31 kHz, 40 kHz, 50 kHz, 63 kHz, and 79 kHz. The coating sample was tested every day. The duration of the evaluation was 11 days. Same experimental condition is applied to the EIS instrument. The result from the EIS instrument is given in figure 23.
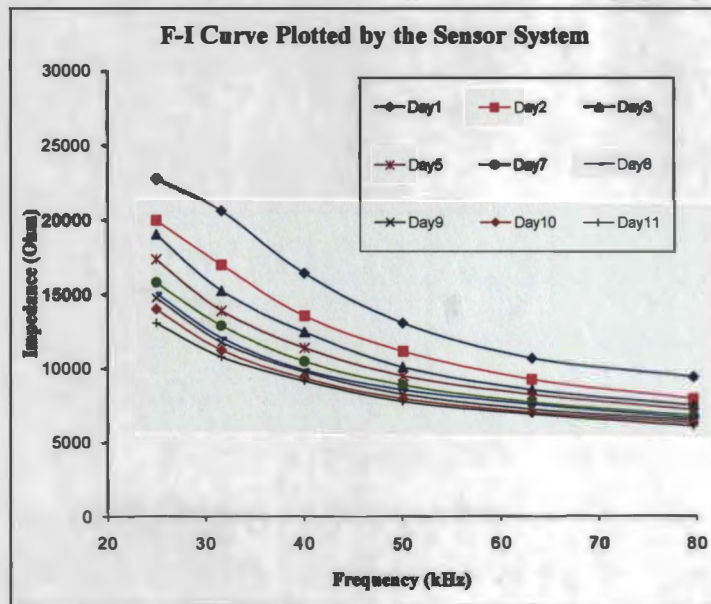
Figure 22. Experiment result for Epoxy Primer + ANAC topcoat obtained by the sensor system

Same f-i curve variation between the results from sensor system and from the EIS instrument is observed. In figures 22 and 23, Day 1 is the first day that coating sample is immersed in the DHS. Impedance on Day 1 is the original impedance for a coating sample with good performance. On Day 2, an obvious impedance drop in the coating f-i curve are observed for both EIS result and sensor system result. This can be inferred as after one day accelerated degradation immersion service in the DHS, the
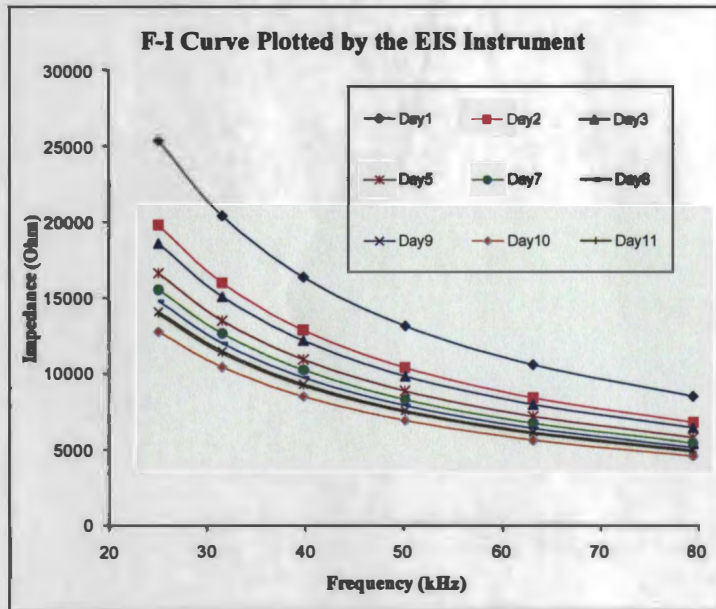
Figure 23. Experiment result for Epoxy Primer + ANAC topcoat obtained by the EIS instrument

protection performance of the coating sample is degraded by the DHS which results in an impedance drop. In the following days, the f-i curve keeps dropping. But the speed of the f-i curve decreasing is much slower compared to the first two days. on Day 10 and Day 11, a very small impedance drop is observed. This indicates the degradation of the coating corrosion resistance level is nearly to the maximum.

After calibration, the impedance variation range obtained from the sensor system and EIS instrument are both from 6 kΩ to 25 kΩ approximately. If a threshold f-i curve can be defined based on the low frequency coating impedance data, a good coating system and a bad coating system can be identified by the sensor system.

4.2.2. Mg-rich Primer

The one component Mg-rich primer has been used for the protection of the Al substrates. Coating evaluation of the Mg-rich primer on an Al plate ($5 \times 5 \times 0.02$ cm^3) was conducted where the coating was subjected to DHS exposure. Evaluation was accomplished using electrodes between the substrate and primer. This coating sample

34

was evaluated both by the sensor system and the EIS instrument. The duration of this experiment was 14 days.

Figure 24 shows the f-i curve variation in terms of immersion time plotted by the sensor system. A similar plot obtained from the EIS instrument is given in figure 25. Compared with the coating system which consists of Epoxy primer and ANAC topcoat, the impedance of the Mg-rich primer is much smaller. The reason is the Mg-rich primer contains metallic particles. These particles increase the electrical conductivity of the coating which results in lower coating impedance.
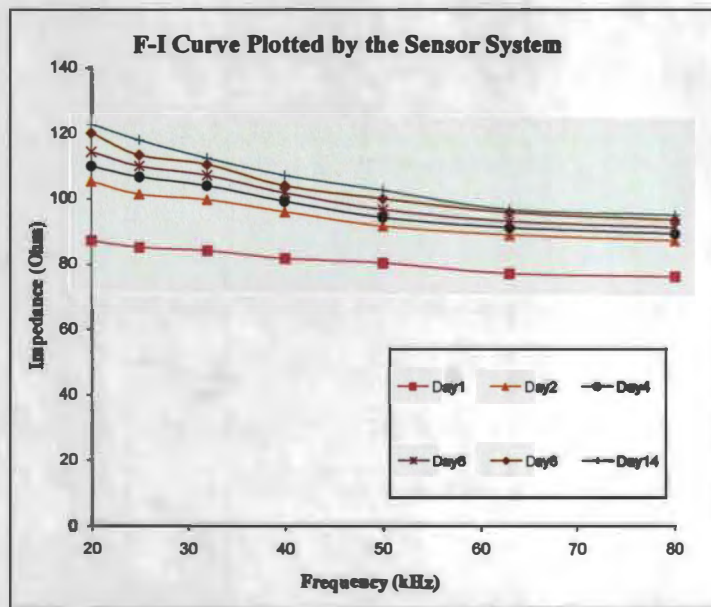
Figure 24. Experiment result for Mg-rich primer obtained by the sensor system

To protect the Al substrate, the Mg-rich primer functions as a barrier to prevent the transport of water, ions, and oxygen from outside environment to substrate. In the process of protection, the magnesium particles are consumed by water, ions, and oxygen in outside environment due to the chemical reaction [4]. This leads the impedance increment because of the reduced conductivity of the Mg-rich primer.

Comparing the f-i curve from the sensor system to the f-i curve from the EIS instrument, similar impedance variation is observed. As shown in figures 24 and 25,

35
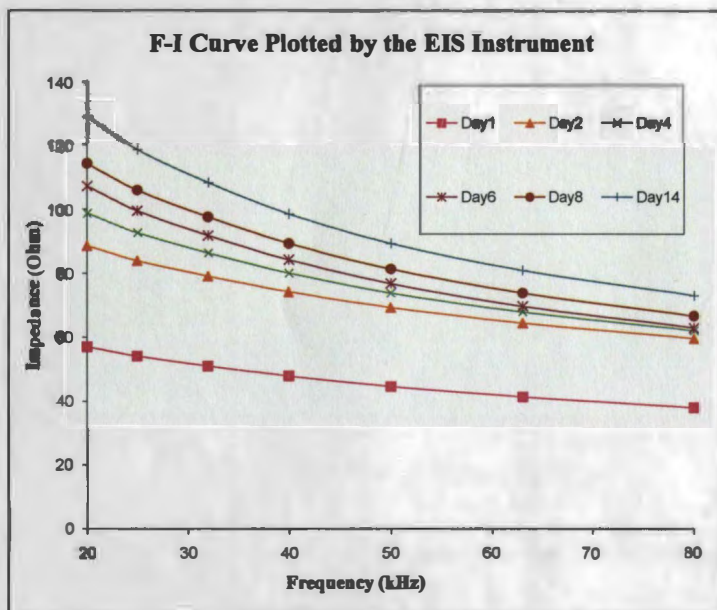
Figure 25. Experiment result for Mg-rich primer obtained by the EIS instrument

the impedance on Day 1 is most closed to the original impedance of the coating. After one day immersion, there is an obvious impedance increment between the Day 1 and Day 2. After Day 2, the impedance increases slower for each measurement. After data calibration, same impedance variation and closed impedance values for EIS results and sensor system results are observed.

4.2.3. Mg-rich Primer +ANAC topcoat

The third experiment in this work was to test a two component coating system which consists of Mg-rich primer and an ANAC topcoat. The coating system was applied on an Al plate ($10 \times 5 \times 0.02$ cm^3). The coating system was immersed in the DHS for accelerated coating degradation purpose. The duration of this experiment was 17 days.

Figure 26 shows the coating f-i curve results from the sensor system. Figure 27 shows the f-i curve results from EIS instrument. In figures 26 and 27, the impedance trend within the frequency range of 20 kHz to 90 kHz is decreased as the immersion time increased. The coating impedance data on Day 1 is the original impedance

36

before the coatings immersed in the DHS. From Day 1 to Day 2, the f-i curve has an obvious decrement, which indicates that the coating protection performance is degraded critically during the first day. However, from the f-i curve from Day 2 to Day 17, only a small decrement is observed. After Day 15, the f-i curve variation of the coatings almost stops since the f-i curve measured on Day 16 and the f-i curve measured on Day 17 have an obvious overlap. This can be explained as a maximum degradation happened in the tested coating sample.
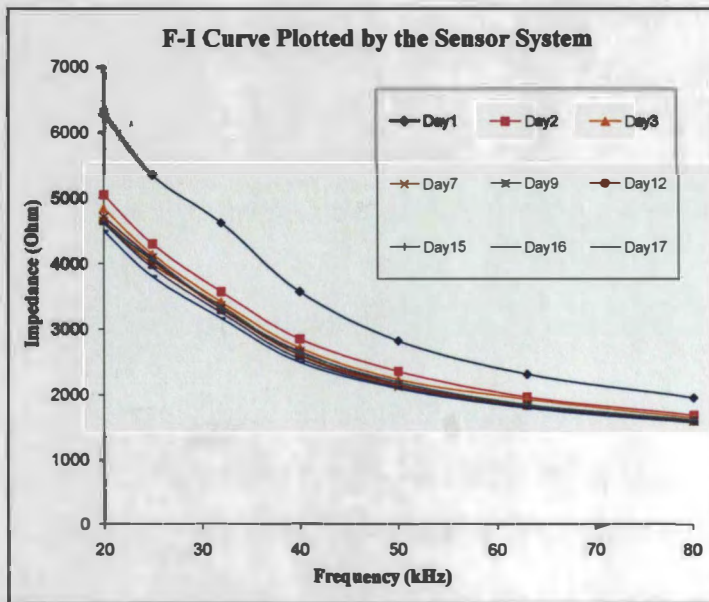
Figure 26. Experiment result for Mg-rich primer and ANAC topcoat obtained by the sensor system

These three experiments provide good correlations on f-i curve measurements in frequency range from 20 kHz to 90 kHz between the sensor system and the expensive commercial EIS instrument. Based on the comparison between the experimental results from the EIS instrument and the experimental results from the sensor system, the proposed sensor system is valid for high frequency coating performance evaluation.
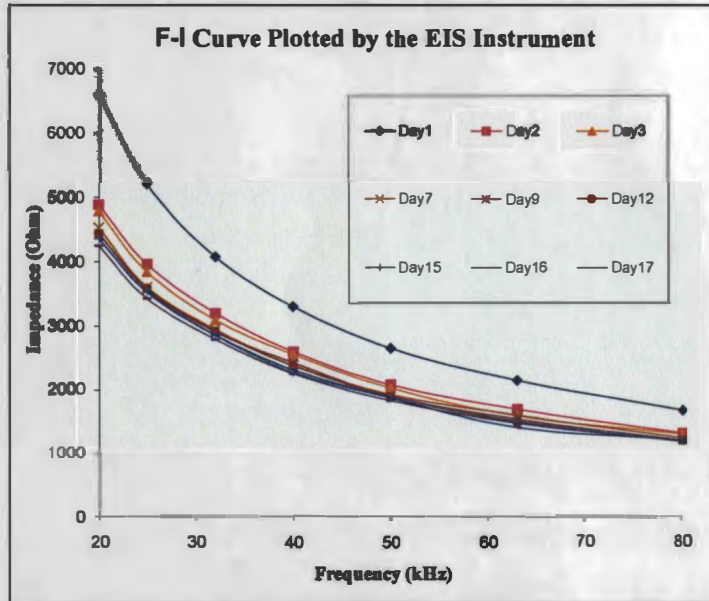
Figure 27. Experiment result for Mg-rich primer and ANAC topcoat obtained by the EIS instrument

4.3. Advantages of the EIS-based Sensor System

Two major traditional methods for coating evaluation are EIS technique and ENM technique. These two techniques both require bulky and expensive equipment. Complicated and expensive electrode connection is not conducive to coating evaluation in the field. The proposed sensor system in this thesis introduces a new technique for coating evaluation in high frequency. The cost of the sensor system is very low ($60) compared to the tradition EIS evaluation which may cost over $4000. The sensor system is powered by batteries. The total power consumption is about 420 mW, which is lower than the commercial EIS instrument. The sensor system is portable. With the wireless communication feature, the sensor system can realize long-distance, remote coating evaluation in the field.

CHAPTER 5. CONCLUSION

Researches on coating evaluation are very important for reducing the business corrosion cost and tackling safety issues. EIS is a traditional technique for coating evaluation. The principle of the EIS-based coating evaluation is to measure the coating impedance in a frequency range. Coating impedance variation indicates the coating performance changes. Traditional EIS coating evaluation measures the coating impedance in the frequency range of 0.01 Hz to 100 kHz. However, low frequency coating impedance variation has the same trend as in a corresponding high frequency range. Based on this idea, the proposed sensor system is designed for coating evaluation in a high frequency range. The sensor system generates its own frequency sweep range, then applies to the coating. The sensor system measures and records the coating impedance, then sends the data to the PC for further data processing. Wireless communication is realized in the sensor system for remote coating evaluation purposes. The micorcontrolle based sensor system design not only reduces the sensor prototype size, but the power consumption is also lowered. The feasibility of the proposed sensor system is proved by the good correlations between EIS instrument experimental results and sensor system experimental results. Compared to the commercial EIS instrument, the proposed sensor system has much lower cost and lower power consumption. In addition, wireless communication feature realizes the in field long distance coating evaluation which is hard to be achieved by the commercial EIS instrument.

In the future, a wireless sensor network can be designed. With an optimal two way wireless communication protocol, the base station can communicate with multiple sensor nodes simultaneously. The sensor system can thereby conduct multi-location coating evaluation in field. In addition, the sensor node can be integrated into a chip based on the integrated circuit design techniques. The power consumption

and the size of the sensor node will then be further reduced.

REFERENCES

[1] V. S. Agarwala, P. L. Reed, and S. Ahmad, *Corrosion detection and monitoring - a review*, CORROSION 2000, Orlando, Fl, Mar. 2000.

[2] K. N. Allahar, D. Wang, D. Battocchi, G. P. Bierwagen, and S. Balbyshev, *Real-time monitoring of an air force topcoat/mg-rich primer system in b117 exposure by em- bedded electrode*, Corrosion Science, Atalanta, GA, Mar. 2009.

[3] R. C. Bacon, J. J. Smith, and F. M. Rugg, *Electrolytic resistance in evaluating protective merit of coatings on metals*, Ind. Eng. Chem. **40** (1948), 161–167.

[4] G. Bierwagen, *The next generation of aircraft coatings systems*, Proceeding of the XXVth FATIPEC Congress (Turin, Italy), vol. I, September 2001, pp. 1–21.

[5] G. Bierwagen, J. Li, L. He, and D. Tallman, *Fundamentals of the measurement of corrosion protection and the prediction of its lifetime in coatings*, in Proceedings of the 2nd International Symposium on Service Life Prediction Methodology and Metrologies, Monterey, CA, Nov. 1999, pp. 14–17.

[6] G. P. Bierwagen, X. Wang, and D. E. Tallman, *In situ study of coatings using embedded electrodes for enm next term measurements*, Progress in Organic Coatings **46** (2003), 163–175.

[7] K. D. Conners, W. J. Van Ooij, D. J. Mills, and G. P. Bierwagen, *Comparison of electrical impedance spectroscopy and electrochemical noise measurement of plasma polymerized films as pretreatment for coldrolled steel*, British Corrosion, Journal of **35** (2000), 141–144.

[8] Datasheet, *74ls92*, Motorola, http://www.motorola.com/Consumers/US-EN/GLP.

[9] V. Crdenes Van den Eynde, R. Paradelo, and C. Monterroso, *Passivation techniques to prevent corrosionnext term of iron sulphides in roofing slates*, Corrosion Science **51** (2009), 2387–2392.

[10] L. Fu, K. A. Khor, H. W. Ng, and T. N. Teo, *Non-destructive evaluation plasma sprayed functionally graded thermal barrier coating*, Surface and Coatings Technology **130** (2000), 233–239.

[11] L. G. Gray and B. R. Appleman, *Eis: Electrochemical impedance spectroscopy: A tool to predict remaining coating life?*, Journal of protective coatings & linings **20** (2003), no. 2, 66–74.

[12] E. S. Ibrahim, *Corrosion controlnext term in electric power systems*, Electric Power Systems Research **52** (1999), 9–17.

[13] K. Juttner and W. J. Lorenz, *Electrochemical impedance spectroscopy (eis) of corrosion processes on inhomogeneous surfaces*, Electrochimica Acta **35** (1990), 1501–1508.

[14] P. Kern, A. L. Baner, and J. Lange, *Electrochemical impedance spectroscopy as a tool for investigating the quality and performance of coated food cans*, Journal of Coatings Technology **71** (1999), 67–74.

[15] H. L. Krauss, C. W. Bostian, and F. H. Raab, *Solid state radio engineering*, Wiley, John & Sons, Incorporated, 1980.

[16] V. A. Tyagai N. B. Lukyanchikova, *Electrochemical noise of reversible electrode reactions*, Electrochimica Acta **18** (1973), 229–230.

[17] S. Mabbutt, D.J. Mills, and C.P. Woodcock, *Developments of the electrochemical noise method (enm) next term for more practical assessment of anti-corrosion coatings*, Progress in Organic Coatings **59** (2007), 192–196.

[18] D. D. Macdonald, *Reflections on the history of electrochemical impedance spectroscopy*, Electrochimica Acta **51** (2004), 1376–1388.

[19] Application node, *Eis pc4 instrument appliocation note*, Gamry Instruments, www.gamry.com.

[20] M. O'Donoghue, R. Garrett, V. Datta, P. Robert, and T. Aben, *Electrochemical impedance spectroscopy: testing coatings for rapid immersion service*, Materials Performance **42** (2003), 34–61.

[21] Mike ODonoghue, R. Garrett, and V. J. Datta, *Eis investigations of alkyd and epoxy coatings as they are chemically stripped from steel panels*, Corrosion **42** (2003), 31–60.

[22] N. Polydoridesa, G. E. Georghiou, D. H. Kim, and C. Won, *Subspace constrained regularization for corrosion detectionnext term with magnetic induction tomography*, NDT & E International **41** (2008), 510–516.

[23] R. L. De Rosa, D. A. Earl, and G. P. Bierwagen, *Statistical evaluation of eis and enm next term data collected for monitoring corrosion barrier properties of organic coatings on al-2024-t3*, Corrosion Science **44** (2002), 1607–1620.

[24] R. L. De Rosa, J. T. Grant, L. Kasten, M. Donley, and G. P.Bierwagen, *Surface analysis of various methods of preparing al 2024 t-3 surface for painting*, Corrosion **56** (2000), 395–400.

[25] I. Sekine, M. Yuasa, N. Hirose, and T. Tanaki, *Degradation evaluation of corrosion protective coatings by electrochemical, physicochemical and physical measurements*, Progress in Organic Coatings **45** (2002), 1–13.

[26] Data sheet, *Pic16f876*, Microchip, http://www.microchip.com/.

[27] G. E. Simmers, *Impedance-based structural health monitoring to detect corrosion*, Master's thesis, Virginia Tech, 2005.

[28] Q. L. Thu, G. P. Bierwagenb, and S. Touzain, *Eis and enmnext term measurements for three different organic coatings on aluminum*, Progress in Organic Coatings **42** (2001), 179–187.

[29] V. A. Tyagai and N. B. Lukyanchikova, *Electrochemical noise of iodine reduction on a cadmium sulfide surface*, Sueface Science **12** (1968), 331–340.

APPENDIX A. SOURCE CODE FOR THE SENSOR NODE DESIGN

```
#include   <pic.h>
#include   <math.h>
#include   <stdio.h>
#include   "function.h"
#include   "function.c"
#include   "bootloader.c"


static  volatile  int  Comp1            @ 0x15;
static  volatile  int  Comp2            @ 0x1B;
static  volatile  int  TIMER1_L         @ 0x0E;


static  volatile  unsigned  long  int  N,  Fq,  Temp,  ;
static  volatile  unsigned  long  int  a,  b,  A2D_result;
static  volatile  unsigned  int  i,  j,  Res_counter,  time;



int  A2D_Read(unsigned  int  N)
{
char  i;
int  result;
ADCON0 = 0x81 + (N << 3);
for (i=0; i<14; i++);
ADGO=1;
while(ADGO);
```

```c
result= (ADRESH<<8)+ADRESL;
return(result);
}



void SCI_Out(unsigned long int DATA, unsigned int DOT)
{
unsigned int A[8], i;
for (i=0; i<8; i++)
        {
        A[i] = DATA % 10;
        DATA = (DATA - A[i]) / 10;
        }
while(!TRMT);   TXREG = A[7] + '0';
while(!TRMT);   TXREG = A[6] + '0';
while(!TRMT);   TXREG = A[5] + '0';
while(!TRMT);   TXREG = A[4] + '0';
while(!TRMT);   TXREG = A[3] + '0';
        if (DOT==1)
        {
        while(!TRMT);   TXREG = '.';
        }
while(!TRMT);   TXREG = A[2] + '0';
while(!TRMT);   TXREG = A[1] + '0';
while(!TRMT);   TXREG = A[0] + '0';
while(!TRMT);   TXREG = ' ';
```

```
}


//-----status checking
void note( )
{
PORTB=0x00 ;
Wait_ms(100);
PORTB=0xFF ;
Wait_ms(100);
}



void SCI_KHz( )
{
while(!TRMT);   TXREG = A2D_result ;
while(!TRMT);   TXREG = 104;
while(!TRMT);   TXREG = 122;
while(!TRMT);   TXREG = ' ';
while(!TRMT);   TXREG = ' ';
}



void SCI_CRLF( )
{
while(!TRMT);   TXREG = 13;
```

```c
while (!TRMT);   TXREG = 10;
}


// Main Routine
void main(void)
{
TRISA = 0b00000111;
TRISB = 0b00000000;
TRISC = 0b00000001;
GIE = 1;// enable global interrupt
PEIE=1;// for interrupt
time=10;//testing speed adjustment;


//Initial A2D
ADCON0=0x81;
ADCON1=0x80;


// Timer2 Setup
TMR2IE = 0;// 1 Enable, 0 Disable
TMR2ON = 0;   // 1 Enable, 0 Disable
PR2 = 249;
T2CON = 0x4D; // include set T2E!!
TMR1IE=0;
```

```c
TMR1ON=1;


//----Comp mode setup
CCP1IE =1;
CCP1CON=0x08;
CCP1M0=0;
CCP1M1=1;
Comp2=0;
Comp1=0;


// Serial Port at 115k bps
TRISC = TRISC | 0xC0;
TXSTA = 0x22;
RCSTA = 0x90;
TXIE = 0;
RCIE = 0;
BRGH = 1;
SPBRG = 10;
SYNC = 0;


while (RC0==0)
{
SCI_CRLF();
```

```
SCI_CRLF ( ) ;
for  (Fq=2000;  Fq<=10000;  Fq=Fq+80)
          {
          SCI_CRLF ( ) ;
          PORTB  =  0x00 ;
          N=5000000/(2*Fq) ;
          ADCON0  =  0x89 ;
          a  =  A2D_Read ( 2 ) ;
          SCI_Out ( Fq*12 ,0 ) ;
          SCI_Out ( a , 0 ) ;
          tx_data ( ) ;
          }
SCI_CRLF (  ) ;
}
}




//----------interrupt  operation----------------
void  interrupt  IntServe ( void )
{
          if  (CCP1IF==1)
          {
          Comp1  +=  N;
          RC4  =  !RC4;
          CCP1IF=0;
```

```
        asm(" clrwdt ");

        }

}
```

APPENDIX B. SOURCE CODE FOR THE BASE STATION DESIGN

```c
#include <pic.h>
#include <stdio.h>
#include "function.c"
#include "bootloader.c"


static volatile long int a,b,c;
static volatile unsigned int i, j, aL, aH;
static volatile unsigned int result, reader, time;


//-----SCI setup
void SCI_Out(unsigned long int DATA, unsigned int DOT)
{
unsigned int A[8], i;
for (i=0; i<8; i++)
        {
        A[i] = DATA % 10;
        DATA = (DATA - A[i]) / 10;
        }
while(!TRMT);   TXREG = A[7] + '0';
while(!TRMT);   TXREG = A[6] + '0';
while(!TRMT);   TXREG = A[5] + '0';
while(!TRMT);   TXREG = A[4] + '0';
while(!TRMT);   TXREG = A[3] + '0';
        if (DOT==1)
```

```
        {
        while (!TRMT);   TXREG = '.';
        }
while (!TRMT);   TXREG = A[2] + '0';
while (!TRMT);   TXREG = A[1] + '0';
while (!TRMT);   TXREG = A[0] + '0';
while (!TRMT);   TXREG = ' ';
}


void SCI_KHz( )
{
while (!TRMT);   TXREG = 75;
while (!TRMT);   TXREG = 104;
while (!TRMT);   TXREG = 122;
while (!TRMT);   TXREG = ' ';
while (!TRMT);   TXREG = ' ';
}


void SCI_Data( )
{
while (!TRMT);   TXREG = 68;
while (!TRMT);   TXREG = 97;
while (!TRMT);   TXREG = 116;
while (!TRMT);   TXREG = 97;
while (!TRMT);   TXREG = ' ';
while (!TRMT);   TXREG = ' ';
```

```
}


void SCI_CRLF( )
{
while (!TRMT);   TXREG = 13;
while (!TRMT);   TXREG = 10;
}


void test_start( )// test start signal for each bit...
{
L1:  if (reader==1)
        {
        Wait_ms(12);
         }
                else goto L1 ;
                        if (reader==1)
                        {
                        Wait_ms(11);
                        }
                                else goto L1;

}


// --------Main Routine...
void main(void)
{
TRISA = 0b00000000;
```

```c
TRISB = 0b00000000;
TRISC = 0b00000011;
GIE = 1;
PEIE=1;


// Timer2 Setup with interrupt for 1ms, frequency =1 KHz
TMR2ON = 1;                    // 1 Enable, 0 Disable
TMR2IE = 1;
T2CON  = 0x54;
PR2 = 249;


// set baud rate as 115k bps
RISC = TRISC | 0xC0;
TXSTA = 0x22;
RCSTA = 0x90;
TXIE = 0;// no interrupt on transmiter
RCIE = 0; // no interrupt on receiver
BRGH = 1;
SPBRG = 10;
SYNC = 0;
//--main
while(1)
{
if(RC0==1)
{
aL=0x00; aH=0x00; result=0x00;//reset
```

```
read_head();
test_start();aL=reader;
test_start();aL=aL|(reader<<1);
test_start();aL=aL|(reader<<2);
test_start();aL=aL|(reader<<3);
test_start();aL=aL|(reader<<4);
test_start();aL=aL|(reader<<5);
test_start();aL=aL|(reader<<6);
test_start();aL=aL|(reader<<7);
test_start();aH=reader;
test_start();aH=aH|(reader<<1);
result=(long int)(((long int)aH)<<8|aL);
SCI_Out(result,0);
SCI_CRLF();
}
}
}



//----------INTERRUPT----------------
void interrupt IntServe(void)
{
        if (TMR2IF)
        {
        reader=RC1;
        RC2=!RC2;
```

```c
    asm(" clrwdt ");
    TMR2IF=0;
    }
}
```